0888-8809/08/$15.00/0
Printed in U.S.A.

Molecular Endocrinology 22(3):636–648

doi: 10.1210/me.2007-0359

GPR30 Contributes to Estrogen-Induced Thymic Atrophy

Chunhe Wang, Babak Dehghani, I. Jack Magrisso, Elizabeth A. Rick, Edna Bonhomme, David B. Cody, Laura A. Elenich, Sandhya Subramanian, Stephanie J. Murphy, Martin J. Kelly, Jan S. Rosenbaum, Arthur A. Vandenbark, and Halina Offner

Neuroimmunology Research (C.W., B.D., E.B., S.S., A.A.V., H.O.), Veterans Affairs Medical Center, Portland, Oregon 97239; Departments of Neurology (C.W., B.D., A.A.V., H.O.), Physiology & Pharmacology (E.A.R., M.J.K.), Molecular Microbiology & Immunology (A.A.V.), and Anesthesiology & Peri-Operative Medicine (S.J.M., H.O.), Oregon Health & Science University, Portland, Oregon 97239; and Procter & Gamble Pharmaceuticals (I.J.M., D.B.C., L.A.E., J.S.R.), Mason, Ohio 45040

The mechanisms by which prolonged estrogen exposures, such as estrogen therapy and pregnancy, reduce thymus weight, cellularity, and CD4 and CD8 phenotype expression, have not been well defined. In this study, the roles played by the membrane estrogen receptor, G protein-coupled receptor 30 (GPR30), and the intracellular estrogen receptors, estrogen receptor α (ERα) and β (ERβ), in 17β-estradiol (E2)-induced thymic atrophy were distinguished by construction and the side-by-side comparison of GPR30-deficient mice with ERα and ERβ gene-deficient mice. Our study shows that whereas ERα mediated exclusively the early developmental blockage of thymocytes, GPR30 was indispensable for thymocyte apoptosis that preferentially occurs in T cell receptor β chain$^{-/low}$ double-positive thymocytes. Additionally, G1, a specific GPR30 agonist, induces thymic atrophy and thymocyte apoptosis, but not developmental blockage. Finally, E2 treatment attenuates the activation of nuclear factor-κ B in CD25$^-$CD4$^-$CD8$^-$ double-negative thymocytes through an ERα-dependent yet ERβ- and GPR30-independent pathway. Differential inhibition of nuclear factor-κB by ERα and GPR30 might underlie their disparate physiological effects on thymocytes. Our study distinguishes, for the first time, the respective contributions of nuclear and membrane E2 receptors in negative regulation of thymic development. (*Molecular Endocrinology* 22: 636–648, 2008)

EXTENDED SEX STEROID exposures, such as that which occurs during estrogen therapy and pregnancy, lead to thymic atrophy and loss of cellularity in both humans and animals (1–5). Thymic atrophy triggered by estrogens might contribute to sexual dimorphism in the immune response and susceptibility to autoimmune disease (6, 7), as well as down-regulation of autoimmune responses (8) and maternal tolerance toward the fetus during pregnancy (9). However, the mechanism by which estrogens reduce the thymus size and cellularity remains elusive.

It was traditionally believed that estrogens exert most, if not all, of their pleiotropic effects by binding to intracellular receptors, including estrogen receptor (ER)α (or Esr1), and ERβ (or Esr2) (10). Studies with ERα- and ERβ-knockout (AERKO and BERKO) mice indicate that ERα only partially mediates the regulatory effect of estrogens on thymus (11), whereas ERβ is not generally relevant (12). Together, these studies suggest a possible contribution from another receptor pathway in 17β-estradiol (E2)-induced thymic atrophy. Recently, G protein-coupled receptor 30 (GPR30) (13) has been recognized as a putative membrane receptor for estrogens that mediates a series of nongenomic signals from estrogens (14). Whether GPR30 serves as the other receptor for estrogens in this important biological process is of interest.

In this study, we generated GPR30-knockout (*Gper*$^{-/-}$, GPR30KO) mice, which in combination with AERKO and BERKO mice, were used to evaluate how E2 (the primary estrogen in women from menarche to menopause) effects thymocyte development and apoptosis. We found that the E2-induced developmental block of CD44$^+$CD25$^-$ CD4 and CD8 double-negative (DN) thymocytes was mediated primarily through ERα, whereas E2-induced apoptosis of T cell receptor (TCR)$\beta^{-/low}$ CD4 and CD8 double-positive (DP) thymocytes was mediated primarily through GPR30. Importantly, thymic atrophy was influenced by both ERα and GPR30. Moreover, we found that E2 activation

First Published Online December 6, 2007

Abbreviations: 7AAD, 7-Amino-actinomycine D; Ab, antibody; AERKO, ERα-knockout; APC, Allophycocyanin; BERKO, ERβ-knockout; $[Ca^{2+}]_i$, intracellular calcium; DN, double negative; DNase I, deoxyribonuclease I; DP, double positive; E2, 17β-estradiol; ER, estrogen receptor; ES, embryonic stem; FACS, fluorescence-activated cell sorting; FITC, fluorescein isothiocyanate; GPR30, G protein-coupled receptor 30; KO, knockout; MACS, automated magnetic cell sorting; PE, Phycoerythrin; RT, reverse transcriptase; TCR, T cell receptor; TUNEL, terminal deoxynucleotidyl transferase dUTP nick end labeling; WT, wild type.

***Molecular Endocrinology* is published monthly by The Endocrine Society (http://www.endo-society.org), the foremost professional society serving the endocrine community.**

through ERα, but not ERβ or GPR30, caused inhibition of NFκB in $CD25^-$ DN thymocytes. These data are the first to demonstrate separable signaling pathways through which E2 induces both thymocyte developmental blockage and apoptosis, both of which contributed to thymic atrophy.

RESULTS

Construction and Backcross of GPR30KO Mice

Previous studies reported that E2-induced thymic atrophy is not affected by genetic disruption of ERβ and is only partially reduced in ERα-deficient mice (11, 12), suggesting that an additional E2 receptor pathway might be involved in this process. To investigate whether GPR30, a recently identified membrane receptor for estrogen, plays a role in thymic atrophy, we constructed GPR30-deficient mice as described in *Materials and Methods*. Briefly, *Gper*, the gene encoding GPR30, was targeted in 129 SvEvTac embryonic stem (ES) cells by specific vector with Neo^r insertion (Fig. 1). Initial ES cell screening was conducted using the 3′-probe, which was subcloned as a 1067 bp *Kpn*I/*Apa*I fragment into *Kpn*I/*Apa*I of pGEM7 (Fig. 2A). Restriction digestion with *Hin*d III yields a 6.9-kb band in the wild-type (WT) allele, and a 4.7-kb band in the targeted (Tgt) allele. More than 300 ES cell clones were screened, and a single (+) clone containing both expected bands, denoted T142, was isolated. This clone was subsequently reanalyzed using both probes. The 5′-probe was subcloned as a 1004-bp *Nsi*I/*Stu*I fragment into *Pst*I/*Eco*RV of pBlueScript II. Restriction digestion with *Eco*RI yielded a 10.6-kb band in the WT and 8.2 kb in the Tgt allele, as expected. Restriction digestion with either *Sac*I or *Bam*HI and use of the 3′-probe, respectively, yielded bands of either 7.7 kb or 6.2 kb for the WT allele, and 5.5 kb or 8.2 kb for the Tgt allele, all as expected.

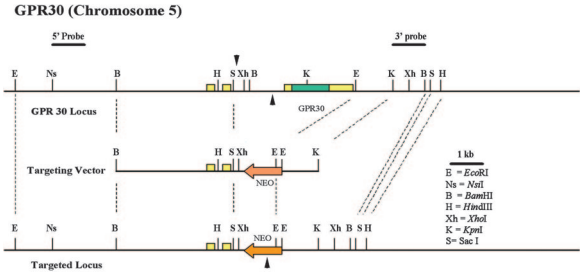

Fig. 1. Schematic Organization of GPR30 Exon Structure and Targeting Strategy

Coding and noncoding exons of GPR30 are indicated by *green and yellow boxes*, respectively. Probes used for Southern blot analyses and their location are labeled and indicated by *solid black bars above* the schematized genomic locus. The positions of PCR primers for genotyping are labeled with *black arrowheads*. Neo, neomycin.

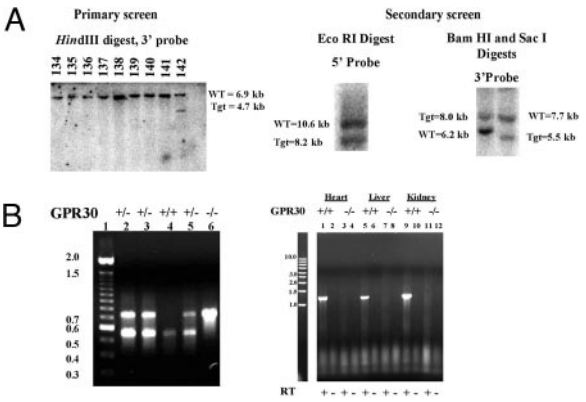

Fig. 2. Validation of Gene Targeting by Southern Blot and Genotyping

A, Southern blot analyses of ES cell genomic DNA. Blotting yields a 6.9-kb band for the WT allele, or 4.7 kb for the targeted allele. A single positive clone, T142, was identified after screening approximately 300 ES cell clones. Both 5′- and 3′-probes were then used with secondary digests to confirm clone T142. B, PCR genotyping. *Left panel*, Genotyping of an initial litter of pups from a heterozygous cross. WT mice yield a 550-bp band upon genotyping, whereas gene-deficient mice yield a 730-bp band. *Right panel*, Confirmation of lack of expression for GPR30 in gene-deficient mice in selected tissues. Total RNA was isolated from heart, liver, and kidney, and RT-PCR was performed with (RT+) or without (RT−) reverse transcriptase. Lanes 1–2, 5–6, 9–10: WT RT(+) and RT(−) reactions; lanes 3–4, 7–8, and 11–12: gene-deficient RT(+) and RT(−) reactions.

The targeted ES cells were microinjected into C57BL/6 blastocysts, which were then implanted into recipient pseudo-pregnant CD1 female mice. Chimeric male mice with high ES cell contribution were then backcrossed to C57BL/6 females. The successful gene targeting was demonstrated by genotyping PCR and Southern blot (Fig. 2B). Mice homozygous for GPR30KO are viable and fertile and do not display any gross physical, immunological, reproductive, or neurological abnormalities. GPR30KO and the WT control mice used in this experiment were backcrossed with C57BL/6J mice six times before breeding with homozygous breeders.

E2-Induced Thymic Atrophy Involves Both ERα and GPR30, But Not ERβ

Before investigating the contribution of different ERs, we first established our thymic atrophy model in WT 8- to 10-wk-old female C57BL/6J mice by implanting s.c. E2 pellets (2.5 mg/60 d release). RIA demonstrated that the serum levels of E2 in treated mice were consistently around the late-stage pregnancy level (data not shown). As shown in Fig. 3A, thymic atrophy occurred as early as the second day after E2 implantation and reached its maximum level 8 d after implantation, as judged by the loss of thymus size, weight, and cellularity. In contrast to thymi, the spleens of the treated mice were abnormally enlarged. To rule out the

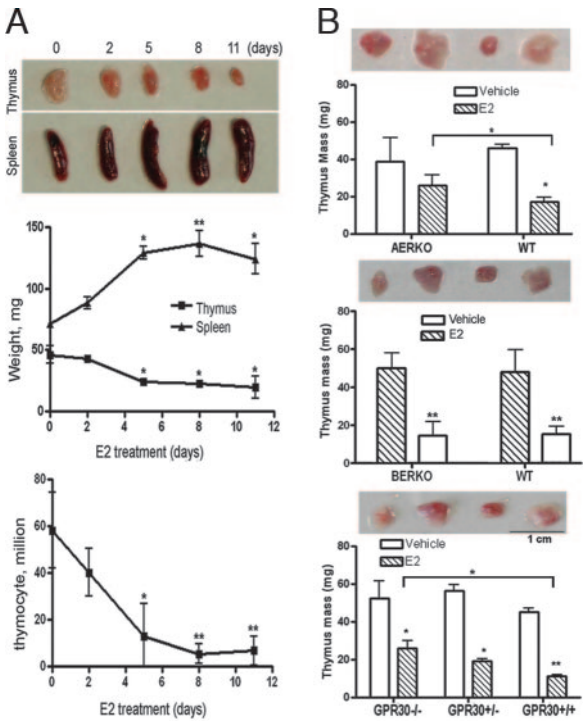

Fig. 3. E2-Induced Thymic Atrophy Involves Both ERα and GPR30, But Not ERβ

A, *In vivo* exposure to pregnancy levels of E2 reduced thymic size and cellularity. Thymi were harvested from female C57BL/6J mice implanted with E2 pellets (2.5 mg/60 d release) for 0–11 days. B, E2-induced thymic atrophy was partially attenuated in both ERα- and GPR30-, but not in ERβ-deficient mice. AERKO, BERKO, GPR30KO, and WT C57BL/6J mice were treated with pellets of E2 (2.5 mg/60 d release) or vehicle for 8 d before thymi were harvested and examined. *, $P < 0.05$; or **, $P < 0.01$, compared with vehicle control as indicated by one-way ANOVA followed by Newman-Keuls multiple comparisons test. The experiment was repeated three times with at least four mice in each group, with a representative experiment shown.

possibility that the E2 treatment may affect the body weight of treated mice, which may in turn impact the overall interpretation of the result, we implanted six WT B6 mice with 2.5 mg/60 d release E2 pellets and another six with vehicle and measured their body weights after 17 d. This pilot study showed that the gross body weight of the mice was not significantly affected by E2 within our treatment time frame (data not shown). Thus, our model provides a relevant platform for investigating the mechanism of E2-induced thymic atrophy.

We then measured the degree of thymic atrophy in AERKO, BERKO, GPR30KO, and WT mice after 8 d of implantation. As reported previously, thymic atrophy was attenuated in AERKO mice, but not completely obliterated (Fig. 3B). Similar to AERKO mice, E2-treated GPR30KO mice showed significantly alleviated, but not completely reversed, thymic atrophy. There was no detectable difference between E2-treated BERKO and WT mice. These results suggested that ERα and GPR30, but not ERβ, played partial roles in E2-induced thymic atrophy.

ERα Mediates Thymocyte Development Blockage at the CD44$^+$CD25$^-$ DN Stage

To investigate the mechanisms by which ERα and GPR30 contribute to thymic atrophy, we studied the cellular events that may lead to thymic atrophy in WT C57BL/6J mice. On the basis of the presence of CD4 and CD8 coreceptors, the maturation of $\alpha\beta$-T cells can be divided into three distinct stages: DN, DP, and single-positive (SP) stages (15). The DN stage can be further divided according to the expression levels of CD44 and CD25: CD44$^+$CD25$^-$ (DN1), CD44$^+$CD25$^+$ (DN2), CD44^{low}CD25$^+$ (DN3) and CD44$^-$CD25$^-$ (DN4) (16–18). Similar to previous reports (3, 19), we found that E2 treatment caused elimination of DP and rapid accumulation of CD4$^-$CD8$^-$ DN thymocytes (data not shown). We went further to determine which CD44- and CD25-expressing DN cells were most affected by E2 treatment. We compared the distributions instead of the absolute cell numbers of specific populations because the latter varies vastly from thymi with different sizes. Figure 4A shows that in normally developing thymi harvested from vehicle-treated controls, about 9.78, 4.71, and 32.13% of the CD3$^-$CD4$^-$CD8$^-$ thymocytes were at DN1, DN2, and DN3 stages, whereas after 8 d of E2 treatment, the DN2 and DN3 thymocytes were sharply reduced to only 0.49% and 2.08% of the total DN thymocytes. Conversely, the DN1 thymocytes were drastically increased from 9.78% to 45.67%. Figure 4B shows the time courses of E2-induced DN thymocyte distribution changes. The decrease of thymocytes at DN2 and DN3 and the increase of DN1 thymocytes suggested that the development of DN cells might be blocked at the DN1 stage.

In AERKO mice, E2-induced accumulation of DN1 and reduction of DN2 thymocytes (Fig. 4C) were completely abrogated. In contrast, genetic disruption of ERβ or GPR30 has no effect on E2-induced developmental blockage of DN thymocytes. Therefore, it is ERα that mediates thymocyte development blockage at the CD44+CD25− DN stage. Notwithstanding, the presence of ERα might be necessary for normal development of DN thymocytes because the percentage of CD44$^+$CD25$^+$ cells in AERKO mice is significantly less than that in WT mice.

GPR30 Enhances Apoptosis in TCR$\beta^{-/low}$ DP Thymocytes

We next assessed the existence of apoptosis in thymus by Annexin V staining of thymocytes (Fig. 5A) and *in situ* terminal deoxynucleotidyl transferase dUTP nick end labeling (TUNEL) staining of thymic sections (Fig. 5B). The results revealed a basal degree of apoptosis existing in the normal thymus (5.12% by Annexin V staining and 137 $\pm$ 54 cells/mm^2 by TUNEL

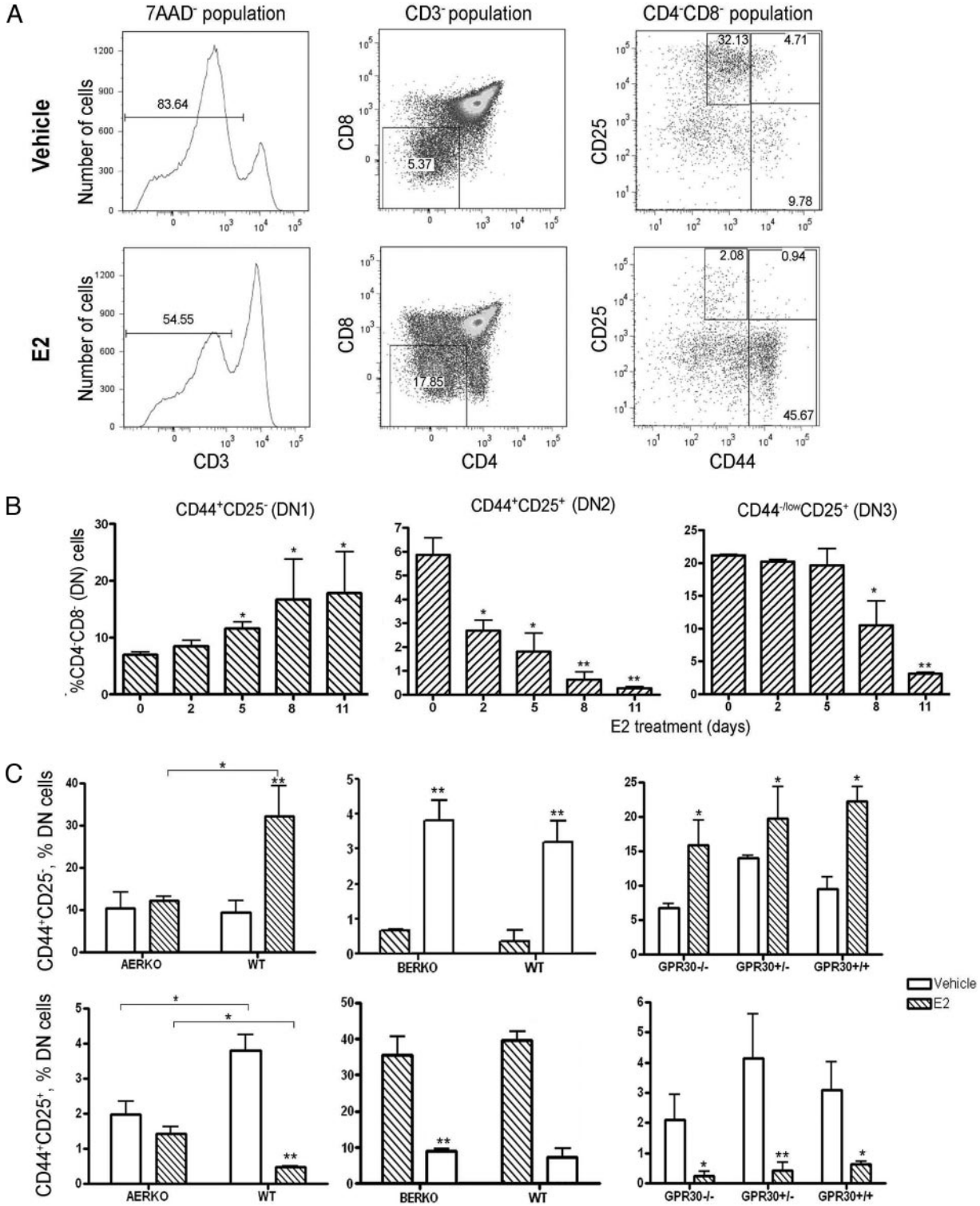

Fig. 4. E2-Dependent Blockage in the Development of DN Thymocytes at the $CD44^{+}CD25^{-}$ (DN1) Stage Was Abrogated in ERα-Deficient Mice

A, *Histogram* and *dot plots* show differential distribution of DN thymocyte subsets in vehicle- and E2-treated mice after 8 d of E2 treatment. B, E2 gradually depleted $CD44^{+}CD25^{+}$ (DN2) and $CD44^{low}CD25^{+}$ (DN3) cells, while enriching $CD44^{+}CD25^{-}$ (DN1) thymocytes during 11 d of treatment. C, Genetic disruption of ERα, but not ERβ or GPR30 expression, abrogated E2-induced accumulation of DN1 thymocytes and reduction of DN2 thymocytes. *, $P < 0.05$; or **, $P < 0.01$, compared with vehicle control as indicated by one-way ANOVA followed by Newman-Keuls multiple comparisons test. The experiment was repeated two times with at least four mice in each group, with a representative experiment shown.

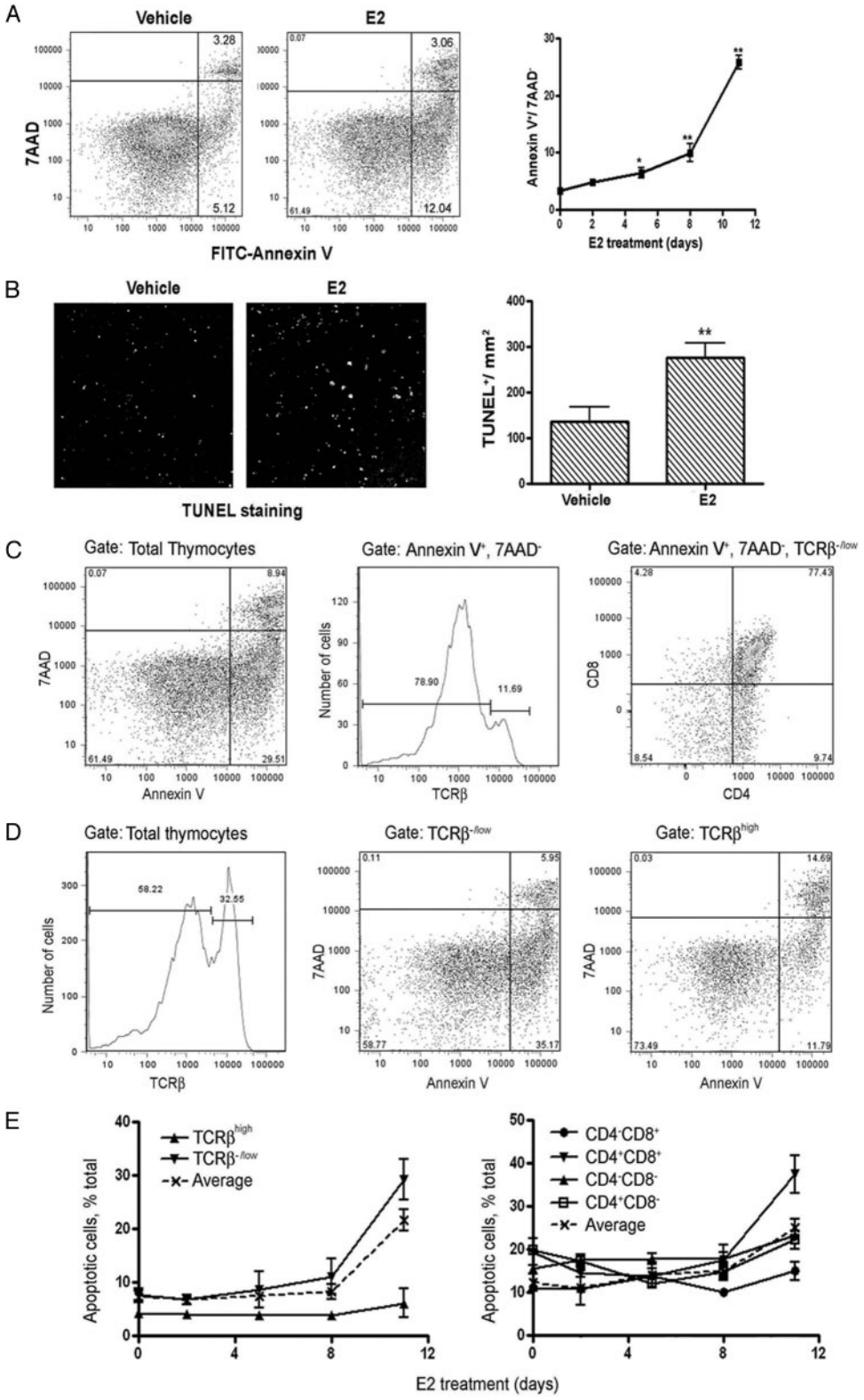

Fig. 5. *In Vivo* E2 Exposure Promoted Apoptosis in TCR$\beta^{-/low}$CD4$^+$CD8$^+$ Thymocytes

A, Annexin V staining shows that thymocyte apoptosis was enhanced by E2 treatment. *Left panel*, *Dot plots* of Annexin V staining in thymocytes prepared from mice implanted with pellets of vehicle or E2 (2.5 mg/60 d release) for 8 d. The apoptotic cells distribute in the Annexin V$^+$7AAD$^-$ *lower right quadrant*. *Right panel*, Time course of E2-induced elevation of apoptotic thymocytes. One-way ANOVA followed by Newman-Keuls multiple comparisons test: *, $P < 0.05$; **, $P < 0.01$, compared with vehicle control. B, *In situ* TUNEL staining showed that E2 treatment elevated apoptosis in the thymus. The number of apoptotic

staining), due possibly to the death and removal of thymocytes that do not pass positive or negative selections. When treated with E2, the number of apoptotic cells more than doubled after 8 d of treatment (12%) and accounted for nearly 30% of thymocytes after 11 d of treatment. Our study further suggested that E2-induced apoptosis was cell type specific, with about 79% of apoptotic cells being TCR$\beta^{-/low}$ and 77% being $CD4^+CD8^+$ DP thymocytes (Fig. 5C). On the other hand, about 35% of the TCR$\beta^{-/low}$ thymocytes were undergoing apoptosis, compared with only 12% of the TCRβ^{high} thymocytes (Fig. 5D). Dynamically, apoptosis developed much faster in TCR$\beta^{-/low}$ and DP populations than in the rest of the thymocytes (Fig. 5E). We thus conclude that E2 treatment preferentially induces apoptosis in TCR$\beta^{-/low}$ DP thymocytes.

In GPR30KO, but not AERKO or BERKO mice, E2-induced apoptosis in TCR$\beta^{-/low}$ DP thymocytes was significantly attenuated (Fig. 6). Thus, whereas ERα accounts for the developmental block of DN thymocytes, GPR30 is indispensable for E2-induced thymocyte apoptosis. It is worthy to note that GPR30 might be antiapoptotic when activated by low concentration of endogenous estrogens because GPR30KO mice showed significantly higher percentage of apoptotic thymocytes (Fig. 6).

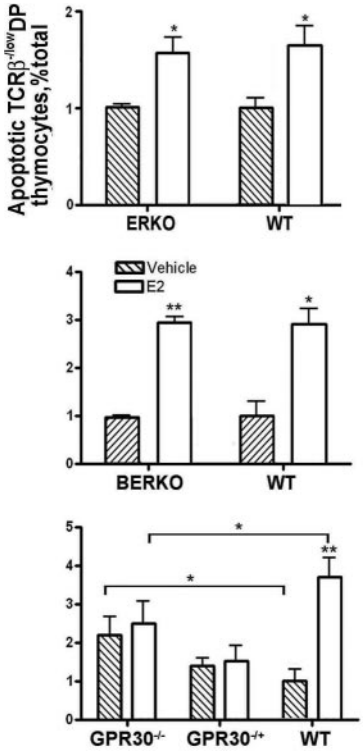

Fig. 6. Genetic Disruption of Expression of GPR30, But Not of ERα or ERβ, Prevented TCR$\beta^{-/low}$ DN Thymocytes from Undergoing Apoptosis

Thymocytes were prepared from mice implanted with pellets of E2 (2.5 mg/60 d release) or vehicle for 8 d. After staining with Annexin V, 7AAD, and Abs for cellular markers, the cells were analyzed by flow cytometry. One-way ANOVA followed by Newman-Keuls multiple comparisons test: *, $P < 0.05$; **, $P < 0.01$, compared with vehicle control or otherwise indicated by *brackets*. The experiment was repeated two times with at least four mice in each group.

GPR30 Agonist Induces Thymic Atrophy and Thymocyte Apoptosis

We next asked whether G1, a synthesized specific agonist for GPR30 (20), could replicate the effect of E2 in thymus. Similar to E2, G1 treatment induced significant thymic atrophy and thymocyte apoptosis (Fig. 7). Interestingly, despite being less effective in inducing thymic atrophy than E2, G1 caused a similar level of thymocyte apoptosis. However, G1 treatment did not block the development of DN thymocytes. Thus, our results with the GPR30 agonist support our conclusion made from using ER-deficient mice.

Differential Inhibition of NFκB by ERα and GPR30

The activation of transcription factors NFκB and NFAT has been shown to be indispensable in the development of DN thymocytes (21) as well as protecting thymocytes from spontaneous apoptosis (22–28). We thus explored the possibility that activation of ERα and GPR30 by E2 inhibits the activity of NFκB and NFAT in thymocytes. After s.c. injection of mice with E2 or vehicle for 8 d, $CD25^-$-DN cells were isolated with automated magnetic cell sorting (MACS) to measure the intrinsic activity of NFκB and NFAT. Figure 8A shows that *in vivo* treatment with E2, but not G1, almost completely abrogated the basal activation of NFκB, whereas neither E2 nor G1 affected the activation of NFAT. These results were further confirmed by immunoblotting of the phosphorylated and total IκB, a protein that releases active NFκB when phosphorylated or degraded (29). We found that IκB phosphorylation was drastically reduced by treatment with E2, but not G1 (Fig. 8B). No change of the protein level of IκB was detected after 8 d of E2 or G1 treatment. Genetic disruption of

cells in TUNEL-stained sections was counted automatically by Scion Image, and the density was calculated by dividing the total number of apoptotic cells by the total area of the sections. Student's *t* test: *, $P < 0.05$; **, $P < 0.01$, compared with vehicle control. The experiment was repeated two times with at least four mice in each group. C, The majority of apoptotic cells were TCR$\beta^{-/low}$ DP thymocytes. B, TCR$\beta^{-/low}$ thymocytes were more vulnerable to apoptosis than TCRβ^{high} thymocytes. C, Apoptosis developed faster in TCR$\beta^{-/low}$ and $CD4^+CD8^+$ (DP) populations. The experiment was repeated four times with at least four mice in each group, with a representative experiment shown.

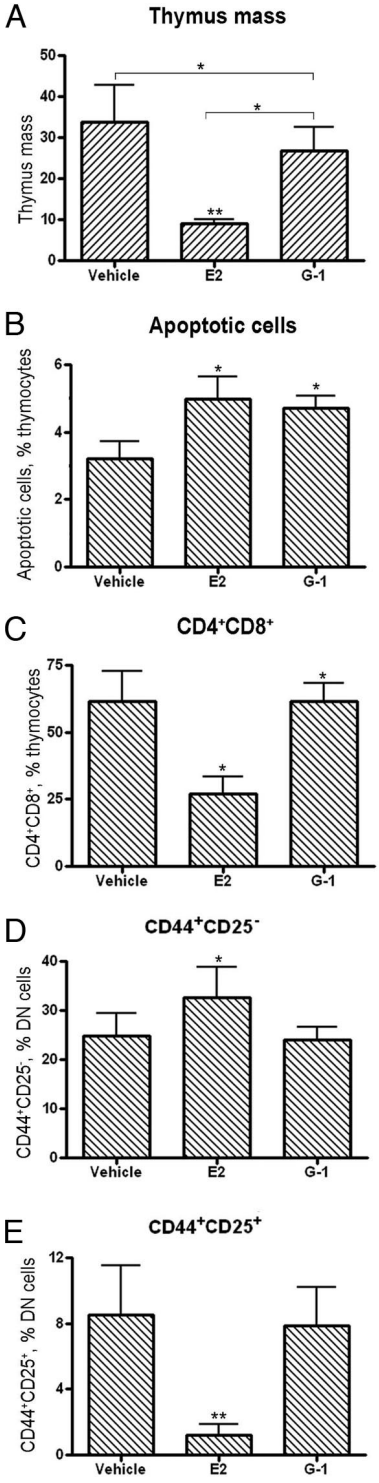

Fig. 7. GPR30 Agonist, G1, Induces Thymic Atrophy (A) and Thymocyte Apoptosis (B). But Not Thymocyte Developmental Blockage (C, D, and E)

E2 (0.04 mg/kg/d) and G1 (0.1 mg/kg/d) were dissolved in vehicle (10% ethanol and 90% oil) and administered sc daily to mice for 8 d before the mice were euthanized to measure the thymic mass, degree of thymocyte apoptosis, and distribution of different DN populations. One-way ANOVA followed by Newman-Keuls multiple comparisons test: *, $P < 0.05$; **, $P < 0.01$, compared with vehicle control or otherwise indicated by *brackets*.

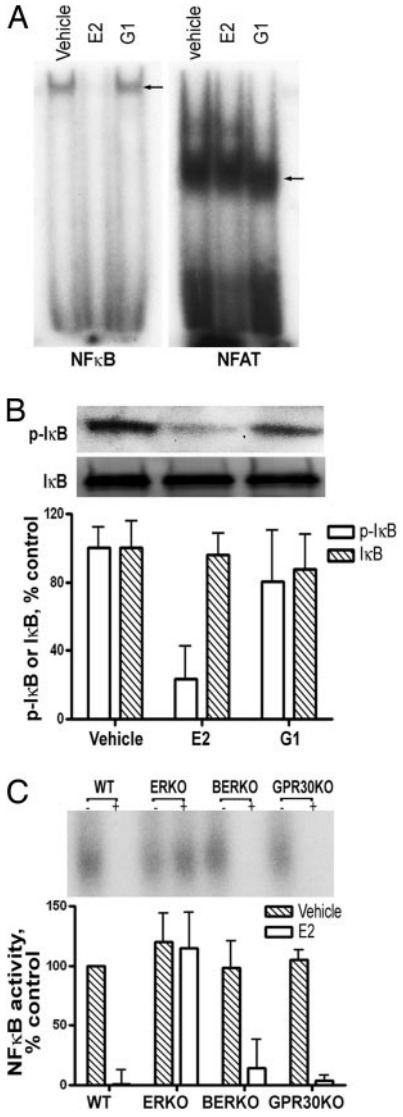

Fig. 8. ERα Mediated E2-Induced Inhibition of NFκB in CD25⁻DN (CD25⁻CD4⁻CD8⁻) Thymocytes

A, The activity of NFκB, but not NFAT, was inhibited by E2, but not G1, in CD25⁻DN thymocytes. CD25⁻DN thymocytes were prepared from C57BL/6J mice that were injected for 8 d sc with E2 (0.04 mg/kg/d), G1 (0.1 mg/kg/d), or vehicle alone. The activity of NFκB and NFAT in CD25⁻DN thymocytes was analyzed with the EMSA. B, The level of IκB phosphorylation was reduced by E2, but not by G1. Cell lysates from CD25⁻DN thymocytes were evaluated by immunoblotting with polyclonal Abs for phosphorylated and total IκB. The bands were scanned and quantified. C, Genetic disruption of expression of ERα, but not ERβ or GPR30, rescued NFκB activity from E2-induced inhibition in CD25⁻DN thymocytes. The activity of NFκB and NFAT in CD25⁻DN thymocytes was analyzed with the EMSA. CD25⁻DN thymocytes were prepared from AERKO, BERKO, GPR30KO, or WT mice. The experiment was repeated two times with four mice in each group.

ERα, but not ERβ or GPR30, prevented E2-induced inhibition of NFκB. Therefore, ERα, but not ERβ or GPR30, mediates E2-induced NFκB inhibition. Dif-

ferential inhibition of NFκB by ERα and GPR30 might underlie the disparate physiological effects of the two types of ERs.

ERα and GPR30 Expression in Thymus

We determined whether the loss of functional GPR30 leads to a change in ERα expression in the thymus or *vice versa* by real-time PCR (Fig. 9A). The fact that a large amount of ERα mRNA was detected in AERKO mice suggests that our TaqMan primer pair from Applied Biosystems (Foster City, CA) is recognizing the truncated and nonfunctional form of ERα in ERKO mice, which is up-regulated by the loss of ERα function. AERKO is known as a functional ERα deletion model (30). As expected, no mRNA of GPR30 was detected in GPR30KO mice. Although the loss of functional ERα resulted in up-regulation of GPR30, suggesting a functional overlap between the two ERs, genetic disruption of GPR30 did not significantly enhance the expression of ERα. Thus, it is unlikely that the undesirable impact on ERα expression by GPR30 disruption contributes to the AERKO-like effects that we observed in GPRKO mice.

Lastly, we studied the expression patterns of ERα and GPR30 in thymocytes at different DN stages. As shown in Fig. 9A, both ERα and GPR30 were expressed in DN2 and DN3 stages, whereas only ERα was expressed in the DN1 stage, and neither receptor was expressed in the DN4 stage. This result suggests that the developmental blocking effect of E2 on DN1 thymocytes may be mediated directly through ERα.

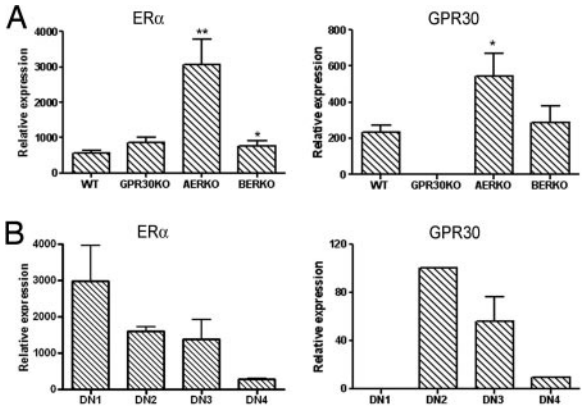

Fig. 9. The Expression of ERα and GPR30 in the Whole Thymus of WT, AERKO, BERKO, and GPR30KO Mice (A) and in the Different CD4$^-$CD8$^-$ (DN) Thymocyte Subsets in WT Mice (B)

For A, the mRNA was extracted from the whole thymus from different phenotypes of mice. For B, the thymocytes were harvested fresh from WT C57BL6 mice and depleted of CD3$^+$ cells by AutoMACS. The thymocytes at different DN stages were then sorted out by flow cytometry. The amounts of mRNA of ERα and GPR30 relative to glyceraldehyde 3-phosphate dehydrogenase (GAPDH) were quantified by real-time PCR using Taqman primers. The experiments were independently repeated two times with two mice in each group. One-way ANOVA followed by Newman-Keuls multiple comparisons test: *, $P < 0.05$; **, $P < 0.01$, compared with vehicle control or otherwise indicated by *brackets*.

DISCUSSION

The composite picture of events that lead to thymus atrophy is not yet clear and merits further study. Whereas some studies suggested that E2 effects may be caused by thymocyte apoptosis (31–33), others reported that E2 delayed the early T cell development in thymus by eliminating almost all CD4$^-$CD8$^-$ DN cells except those that are CD44$^+$CD25$^-$ (3). Zoller and Kersh (19) favored a theory that E2 induces thymic atrophy by eliminating early thymic progenitors in the bone marrow of male mice; however, a follow-up study by the same group found no reduction of bone marrow early thymic progenitors in pregnant female mice (34). Our data presented above showed, for the first time, that both developmental blockage and thymocyte apoptosis coexist in a single model and that both processes, mediated by different classes of ERs, may contribute to the final atrophic outcome. We further showed that the DN cell development was blocked at the CD44$^+$CD25$^-$ stage and that apoptosis occurred mainly in TCR$\beta^{-/low}$ DP thymocytes. These results suggest that E2-induced thymus atrophy is a multidimensional biological process and highlight the pleiotropic nature of the steroid actions.

The roles of classic ERs in thymic atrophy were studied previously by different groups. By using AERKO mice, Staples *et al.* (11) showed that although genetic disruption of ERα abrogates E2-induced DP thymocyte depletion, AERKO mice are still susceptible to E2-induced thymic atrophy, but to a lesser extent when compared with WT mice. Another study using BERKO mice demonstrated that ERβ is not relevant in E2-induced thymic atrophy (12). Thus, a separate signaling pathway might be involved. In this study, we investigated the role played by the putative membrane E2 receptor, GPR30, in E2-induced thymic atrophy.

Genetic disruption of either ERα or GPR30 greatly attenuated E2-induced development blockage or apoptosis, respectively, and significantly alleviated thymic atrophy. Moreover, we showed that ERα, but not GPR30, was expressed in DN1 thymocytes, supporting the idea that the development-blocking effect of E2 in these cells might be mediated directly through ERα. Thus, both ERα-mediated DN thymocyte development blockage and GPR30-mediated apoptosis of TCR$\beta^{-/low}$DP thymocytes serve as possible mechanisms explaining how E2 induces thymic atrophy. However, we cannot conclude that E2-induced thymic atrophy is mediated exclusively by ERα and GPR30. To rule out all other possible contributing pathways would require the construction of ERα and GPR30 double-deficient mice.

GPR30 has been implicated in both positive and negative modulation of apoptotic signaling by *in vitro*

studies. By using an antisense oligonucleotide, Kanda and Watanabe (35) showed that GPR30 may mediate the antiapoptotic effect of E2 in keratinocytes via promotion of Bcl-2 expression and phosphorylating of cAMP response element-binding protein. On the other hand, Kimura *et al.* (36) showed that GPR30 (previously referred to as GPR41) was proapoptotic via a p53/Bax pathway that depends on the HRE (hypoxic response element) in cardiomyocytes. Presently, we show, for the first time, that GPR30 is proapoptotic in the thymus when activated by prolonged exposure to pregnancy levels of E2. However, GPR30 may be antiapoptotic when activated by low level of endogenous E2, because genetic disruption of GPR30 enhances thymic apoptosis in untreated mice. Therefore, the pro- *vs.* antiapoptotic effect of GPR30 may be cell or tissue type and E2 concentration dependent.

Our results from G1-treated WT mice strengthen our conclusions from ER-deficient mice regarding the role of GPR30 in thymus development and the cell types in which GPR30 is acting within the developing thymus. Thus, the same G1 effects in WT mice eliminated the possibility that the observed role of GPR30 in thymic atrophy could be due merely to an artifact of gene deletion or a compensation effect in the developing animal.

Both NFκB and NFAT have been suggested to be involved in the transition of the DN to the DP stage (21). Constitutive activation of transcriptional factor NFκB and NFAT in thymocytes promotes the transition in the DN stages, and inhibition of NFκB or NFAT delays the development of thymocytes from the DN to the DP stage. The transduction of T cell precursors from fetal thymic organ culture with an adenovirus carrying a mutated nondegradable form of IκBα results in a pronounced block in the early stages of T cell development (37). More importantly, transgenic mice expressing a dominant-active form of IκBα exhibit a specific reduction in the absolute number of $CD44^-CD25^+$ and $CD44^-CD25^-$ thymocytes, which normally show high NFκB activity (26). These results set the stage for us to test whether E2 induces thymic atrophy by inhibiting the activation of NFκB and NFAT. The ideal targeting population for our study, certainly, would be the $CD44^+CD25^-$ DN cell population; however, isolation of $CD44^+$ cells would require a touching method that might affect NFκB and NFAT activity. We thus decided to isolate all $CD25^-$DN cells, including $CD25^-CD44^+$ and $CD25^-CD44^-$ DN cells. The result showed that E2 treatment nearly abolished the basal activation of NFκB in $CD25^-$DN cells, an effect that could be reversed by genetic disruption of ERα, but not ERβ or GPR30. Thus, NFκB inhibition is mediated exclusively by ERα and might be the molecular mechanism by which E2 induces the DN cell developmental block and thymic atrophy. However, it is unlikely to be responsible for E2-induced thymocyte apoptosis because GPR30 activation has no effect on NFκB. However, NFκB activity has been shown to protect cells from apoptosis by inducing the expression of antiapoptotic factors, including Bcl-2, Bcl-x_L, A1, and caspase inhibitors (22–25, 38). Thus, the inhibition of NFκB in thymocytes mediated by ERα might make them vulnerable to subsequent GPR30-induced apoptosis. Revankar *et al.* (13) showed that GPR30 potently mobilizes intracellular calcium ($[Ca^{2+}]_i$) when bound to E2. It is possible that prolonged exposure of GPR30 to E2 causes sustained high $[Ca^{2+}]_i$, which in turn leads to apoptosis in NFκB-suppressed thymocytes. Whether GPR30-mediated thymic atrophy can be reversed by constitutive activation of NFκB or negative modulation of $[Ca^{2+}]_i$ in $TCR\beta^{-/low}$ DN thymocytes is an interesting topic for future studies. Finally, we showed that ERα, but not GPR30, was expressed in DN1 thymocytes. Thus, the development-blocking effect of E2 in these cells might be mediated directly by ERα.

Taken together, our results suggest that both ERα-mediated developmental block of $CD44^+CD25^-$ DN thymocytes and GPR30-mediated $TCR\beta^{-/low}$ DP thymocyte apoptosis may contribute to E2-induced thymus atrophy. Our results further indicate that ERα-mediated inhibition of NFκB might be the underlying molecular mechanism. Elucidating the mechanism by which E2 negatively regulates T lymphogenesis will help to better understand gender dimorphism in the immune response and tolerance in the clinical setting.

MATERIALS AND METHODS

Mice

C57BL/6J mice were purchased from The Jackson Laboratory (Bar Harbor, ME). The generation of GPR30- (*Gper*$^{-/-}$, GPR30KO), ERα- (*Esr1*$^{-/-}$, AERKO) and ERβ-deficient (*Esr2*$^{-/-}$, BERKO) mice is described below. All mice used in this study were female, age-matched (8- to 10-wk old), and rested for at least 7 d before the experiment. Animals were housed and cared for according to institutional guidelines in the animal resource facility at the Veterans Affairs Medical Center (Portland, OR).

Reagents

[γ-^{32}P]-ATP, [α-^{32}P]-dCTP and GeneScreen neutral nylon membrane were purchased from PerkinElmer (Waltham, MA). E2 and corn oil was purchased from Sigma-Aldrich (St. Louis, MO). E2 (2.5 mg/ 60 d release) and vehicle (placebo) pellets were purchased from Innovative Research of America (Sarasota, FL). G-1 was purchased from Cayman Chemicals (Ann Arbor, MI). 7-Amino-actinomycin D (7AAD), fluorescein isothiocyanate (FITC)-anti-annexin V, FITC-anti-Sca-1, Phycoerythrin (PE)-anti-CD44, PE-anti-Flt3, Allophycocyanin (APC)-anti-CD3, APC-anti-c-Kit, APC-Alexa Fluor (AF) 750-anti-c-Kit, and PE-cy5-labeled bone marrow lineage markers including CD3, CD4, CD8, Gr-1, TER-119, CD11b, and CD45R were purchased from BD Bioscience (San Diego, CA). Pacific blue-anti-CD4 and PE-cy7-anti-CD25 were purchased from eBioscience (San Diego, CA). Pacific orange-anti-CD8 was from Invitrogen (Carlsbad, CA). The polyclonal antibodies for total and phosphorylated IκB were purchased from Cell Signaling Technology (Danvers, MA). *In Situ* Cell Death Detection Fluorescein kit was product from Roche Applied Science (Indianapolis, IN). NFAT (5′-CGCCC AAAGA

GGAAA ATTTG TTTCA TA-3′) and NFκB (5′-AGTTG AGGGG ACTTT CCCAG GC-3′) probes, and deoxyribonuclease I (DNase I) were purchased from Promega Corp. (Madison, WI). SuperSignal West Pico chemiluminescent kit was purchased from Pierce Chemical Co. (Rockford, IL). Prime-It random primer labeling kit and pMCNeoPolyA and pBluescript II SK (pBSII) plasmids were purchased from Stratagene (La Jolla, CA). Accuprime Supermix II amplification system and Trizol were purchased from Invitrogen. RNeasy kit was purchased from QIAGEN (Valencia, CA). RetroScript kit was purchased from Ambion (Austin, TX). TaqMan Gene expression assay kit and TaqMan primers for GPR30 and ERα were purchased from Applied Biosystems.

GPR30 Targeting Vector Construction

The GPR30KO construct was based on bacterial artificial chromosome RP23–276 B20 from the RPCI-23 female C57BL/6 mouse library, chromosome no. 5. The bacterial artificial chromosome was digested with *Sac*I (as well as *Eco*RV and *Avi*II) and cloned into pBluescript II SK (pBSIISK) plasmid. After Southern colony hybridization, two clones were identified to have the 5′- and the 3′-ends of *Gper* gene. Two intermediate molecules were then made by subcloning into pBSIISK plasmid: one that reconstructed a *Bam*HI-*Kpn*I fragment (site 1), and another into which a *Kpn*I (site 1) to *Kpn*I (site 2) fragment was inserted. All DNA was extensively sequenced to confirm the *in silico* database. The targeting vector was then constructed as follows (Fig. 1): 1) a 1.2-kb fragment from the *Eco*RI site to the second *Kpn*I site (short arm of targeting construct) of mouse GPR30 was cloned into the plasmid pSPORT1 (*Eco*RI/*Kpn* I); 2) a 4-kb fragment from *Bam*HI to *Xho*I (long arm of construct) of *Gper* was then cloned into the *Bam*HI/*Sal*I sites of above intermediate; 3) a blunt-ended *Xho*I/*Sal*I 1.2-kb fragment of pMCNeoPolyA containing the thymidine kinase promoter, the Neo^r gene, and associated polyA sequence was finally cloned into the *Sma*I site just 5′ of the *Gper* short arm and 3′ of the long arm. All cloning junctions were sequenced as a check, and sequencing confirmed the orientation of Neo^r cassette.

ES Cell Screening

SvEvTac ES cells (n = 129) were transfected with the targeting construct via electroporation, and G418-resistant clones were screened by Southern hybridization using probes developed from the 5′- and 3′-ends of the genomic locus outside the recombinant region.

Southern Hybridization

Southern hybridization was conducted using standard alkaline transfer after agarose gel electrophoresis onto GeneScreen neutral nylon membrane. All probes were labeled with [α-^{32}P]-dCTP using the Prime-It random primer labeling kit, and blots were visualized by autoradiography.

Microinjection and Generation of Knockout (KO) Mice

Clone T142 was subsequently microinjected into C57BL/6 blastocysts, which were then implanted into recipient pseudo-pregnant CD1 female mice. Chimeric male mice with high ES cell contribution were then backcrossed to C57BL/6 females; germ line transmission was identified by coat color and then confirmed by Southern hybridization. Female homozygous GPR30-deficient mice (N2) offspring were backcrossed with WT C57BL/6J males from Jackson Laboratory. Their heterozygous progeny (N3) were bred to produce mixed genotypes, and the homozygotic GPR30-deficient animals were selected for breeding a fourth (N4) generation of homozygous *Gper*$^{-/-}$ mice for the present experiments.

PCR Genotyping

Genomic DNA for PCR genotyping analysis was isolated from tail biopsies for all mice with Qiagen DNeasy 96 Tissue kit using a 96-well plate format on a Qiagen BioRobot 3000 automated robotic system. A 3′-primer multiplex assay was developed and executed using Accuprime Supermix II amplification system and the following primers: for the WT and KO animals, the common *Gper* forward (5′-GAGCA CATCT GAGGA GCACT TTGCT GTCTC G-3′) primer was used, respectively, with the Neo reverse (5′-GGATC TCCTG TCATC TCACC TTGCT CCTGC C-3′) and WT *Gper* reverse primer (5′-GTGCC ACCAA CACCC AGCTC ACACA GC-3′). PCR was then executed on a standard thermocycler using the following conditions: initial denaturation, 94 C for 2 min followed by a three-step denaturation-annealing-elongation cycle at 94 C for 30 sec, 62 C for 30 sec, 68 C for 30 sec for 35 cycles. Under these conditions, the common WT forward and WT reverse primers yield a 555-bp band for the WT allele, *vs.* a 730-bp band when the WT forward/ Neo reverse primer was used for the targeted allele.

RT-PCR Expression Analysis and Real-Time PCR

Total RNA was isolated from various tissues for both WT and null mice. Tissues were dissected out and snap frozen in liquid N2, and total RNA was purified using Trizol and RNeasy. After treatment of purified RNA with DNase I to remove any potential genomic DNA, RT-PCR was executed using the RetroScript Kit. Priming of the reverse transcriptase (RT) reactions was performed using random hexamers, followed by amplification for GPR30 using the following primers: Forward: 5′-ATGGA TGCGA CTACT CCAGC CCAAA CTGTT GG3–3′; Reverse: 5′-TCACA CAGCA CTGCT GAACC TGACC TCTGA CTG-3′. PCR amplification using these primers and the cycling conditions outlined for genotyping yield an amplicon of approximately 1.127 kb, which spans the entire coding sequence within the mRNA for GPR30. Control PCRs lacking reverse RT (RT−) were performed for each sample to confirm absence of genomic DNA contamination. Real-time PCR was performed using TaqMan Gene Expression Master Mix and TaqMan primer pairs for GPR30 and ERα from Applied Biosystems. Reactions were conducted on the ABI Prism 7000 Sequence Detection System.

ERα- and ERβ-Deficient Mice

Generation of ERα (*Esr1*)- and ERβ (*Esr2*)-targeted mice is as previously described (30, 39). In these animals, *Esr1* and *Esr2* have been disrupted and are physiologically irresponsive to estrogens by several classical bioassays of estrogenic activity. Both strains originated on a B6;129 background and have been backcrossed to C57BL/6 for at least 10 generations. *Esr1*$^{+/-}$ or *Esr2*$^{+/-}$ breeder pairs were obtained from Dr. Kenneth S. Korach (Laboratory of Reproductive and Developmental Toxicology, National Institute of Environmental Health Sciences, Research Triangle Park, NC). Breeding colonies were maintained using the following breeding harems (two females, one male): *Esr1*$^{+/-}$ harems, *Esr2*$^{+/+}$ (WT) harems, and harems with *Esr2*$^{+/-}$ females and *Esr2*$^{-/-}$ males.

ERα-deficient animals were genotyped by PCR using the following primers in a single reaction: Neo F (5′-GCT GAC CGC TTC CTC GTG CTT TAC), ER 2382 (5′-CGG TCT ACG GCC AGT CGG GCA CC), and mER Intron 2 Rev (5′-CAG GCC TTA CAC AGC GGC CAC CC) (19, 21). The expected sizes of the PCR products are 281 bp for *Esr1*$^{+/+}$ (WT), 760 bp for *Esr1*$^{-/-}$ (KO), and the presence of both PCR products for *Esr1*$^{+/-}$. ERβ animals were genotyped by PCR using the following primers: the intron 2 primer (5′-GTGATGAGCT-GAGGTGGTGCTT-3′), the Neo primer (5′-GCAGCCTCTGT-TCCACATAC-AC-3′), and a third primer from exon 3 (5′-CATCCTTCACAGGACCAGACAC-3′). A 1435-bp band

(intron 2 and exon 3 primers) is amplified for homozygous WT (*Esr2*$^{+/+}$) mice, a 1479-bp band (intron 2 and Neo primers) for homozygous mutant (*Esr2*$^{-/-}$) mice, and both bands for heterozygous (ER$\beta^{+/-}$) mice. Every set of PCRs contained a negative control (no DNA) and a positive control (heterozygous DNA).

Treatments

To investigate the effect of E2 alone, a 3-mm pellet containing 2.5 mg of E2 was implanted sc (dorsally) into mice. These pellets are designed to release their contents at a constant rate over 60 d. Serum levels of E2 were monitored by RIA as described previously (40, 41). For comparison between E2 and G1, both reagents (0.04 mg/kg·d for E2 and 0.1 mg/kg·d for G1) were dissolved in vehicle (10% ethanol and 90% oil) and administered sc daily to mice for 8 d.

MACS

Single-cell suspensions were prepared from thymi after lysis of red blood cells and used for analysis of expression of marker by fluorescence-activated cell sorting (FACS). For EMSA, thymocytes that are negative for CD25, CD4, CD8, and CD3 were isolated and enriched by autoMACS Separator using an untouching method according to the manufacturer's protocols (Miltenyi Biotec, Bergisch Gladbach, Germany). FACS analysis shows that an average of 90–95% purity can be achieved by using this method. Purified cells (2×10^6) were used for the EMSA. For real-time PCR to detect GPR30 expression in thymocytes at different DN stages, the thymocytes were depleted of all CD3$^+$ cells by using Biotinylated-anti-CD3 antibody (Ab) and anti-biotin Ab-coupled beads before flow cytometric sorting.

Flow Cytometry

For regular staining, 1 million (mi) cells were stained at 4 C in the dark with appropriate Ab dilutions in staining buffer (PBS containing 0.5% BSA and 0.02% sodium azide). For analysis of apoptosis, 4 mi cells were first stained with Abs for membrane proteins in staining buffer, and then stained with FITC-Annexin V and 7AAD in binding buffer (10 mM HEPES, pH 7.4; 140 mM NaCl; 2.5 mM $CaCl_2$) according to instruction from BD Biosciences. Flow cytometry data were collected on LSRII and FACSCalibur flow cytometers (BD Bioscience), and analyzed using FlowJo software (Tree Star, Ashland, OR). For flow cytometric sorting, CD3$^+$ cell-depleted thymocytes were labeled with FITC-anti-CD3, FITC-anti-CD4, PE-anti-CD44, APC-anti-CD8, APC-anti-TCRβ, APC-AF750-anti-CD25, and 7AAD. The cell population that is negative for FITC, APC, and 7AAD is sorted into CD44$^+$CD25$^-$ (DN1), CD44$^+$CD25$^+$ (DN2), CD44$^-$CD25$^-$ (DN3), and CD44$^-$CD25$^-$ (DN4) for real-time PCR detection of GPR30 expression.

Immunoblotting

Cells were lysed by incubation with ice-cold radioimmunoprecipitation assay buffer (50 mM Tris-HCl, pH 7.5; 150 mM NaCl; 1% Nonidet P-40; 0.5% deoxycholate; 0.1% sodium dodecyl sulfate; 1 mM $NaVO_3$; and 1× protease inhibitors from Calbiochem, La Jolla, CA) for 15 min with shaking. After centrifugation (14,000 × *g* at 4 C) for 15 min, the supernatant was collected, and the protein concentration was measured and adjusted using radioimmunoprecipitation assay buffer. Samples (30 μl) with equal amounts of protein were mixed with Laemmli loading buffer, denatured at 70 C for 10 min, and separated by SDS-PAGE. The proteins were transferred to polyvinylidene difluoride membrane and visualized with the primary Abs and the SuperSignal West Pico chemiluminescent kit. The intensity of bands was quantified using ImageQuant 5.2 from Amersham Biosciences (Piscataway, NJ).

TUNEL

DNA damage was determined as a means of assessing cell viability using TUNEL assay with *in situ* Cell Death Detection Fluorescein Kit. The kit reagents detect damaged cells *in situ* by specific end labeling and detection of DNA fragments produced by the apoptotic process. The thymi were fixed in 4% paraformaldehyde in buffered saline overnight, embedded in paraffin, and sectioned. The sections were deparaffinized with a standard histological protocol, permeabilized with Triton X-100 at 4 C for 2 min, and then flooded with TdT enzyme and reaction buffer for 60 min at 37°C, followed by direct analysis with a Zeiss fluorescence microscope (Carl Zeiss, Thornwood, NY) equipped with a digital camera to determine the degree of apoptosis. Negative controls were performed by substituting PBS for TdT enzyme in the preparation of working solutions. Positive controls were prepared by treating sections with DNase I for 10 min at room temperature before detection.

EMSA

EMSA was performed as previously described (42). Briefly, thymocytes were homogenized in 0.5 ml of ice-cold lysis buffer containing 20 mM HEPES-KOH, pH 7.6; 420 mM NaCl; 1.5 mM $MgCl_2$; 0.2 mM EDTA; 0.5 mM dithiothreitol; 0.5 Nonidet P-40; 1 mM EGTA; protease and phosphatase inhibitor; and 25% glycerol. The supernatant was saved after centrifuging at 15,000 × *g*, 4 C, for 15 min. The protein concentration was measured with BCA protein assay kit (Pierce, Rockford, IL) and adjusted with an equal volume of lysis buffer. Extracts of 2–4 μg of protein were added into a final volume of 20 μl, which contained 5 μg of polydeoxyinosinic deoxycytidylic acid, 10 mM Tris-HCl (pH 7.5), 0.5 mM EDTA, 5% glycerol, and 2 x 10^4 dpm of [γ-32p]ATP-labeled consensus NFAT or NFκB probes. Mixtures were kept at 37 C for 15 min and were resolved by electrophoresis on 6% DNA retardation gels, which were then exposed to Kodak Biomax MS film (Eastman Kodak, Rochester, NY) at −80 C for overnight. The film was scanned and quantified using ImageQuant 5.2 from Amersham Biosciences.

Statistical Analysis

Mean values from each experiment were compared using one-way ANOVA followed by Newman-Keuls multiple comparisons test or Student's *t* test. Data are represented as mean ± SD. We used at least four mice per treatment group, and all presented data represent one from two to four independent experiments.

Acknowledgments

We thank Ms. Mandy Boyd at the Oregon Health & Science University core facility for technical assistance with flow cytometry; Dr. Kenneth S. Korach, Laboratory of Reproductive and Developmental Toxicology, National Institute of Environmental Health Sciences, Research Triangle Park, North Carolina, for providing ER$\alpha^{+/-}$ and ER$\beta^{+/-}$ (heterozygous) breeder pairs; and Eva Niehaus for assistance in manuscript preparation. We also acknowledge the excellent service and care provided by the Department of Anesthesiology and Peri-Operative Medicine Mouse Colony Core, which oversaw management of the ERα- and ERβ-deficient mouse breeding colonies.

Received July 20, 2007. Accepted November 30, 2007.

Address all correspondence and requests for reprints to: Dr. Chunhe Wang, Neuroimmunology Research R&D-31, 3710 Southwest U.S. Veterans Hospital Road, Portland, Oregon 97239. E-mail address: wangch@ohsu.edu.

This work was supported by National Institutes of Health Grants NS45445, NS49210, and NS38809; National Multiple Sclerosis Society Grants RG3405 and PP1295; The Nancy Davis Multiple Sclerosis Center Without Walls; and the Biomedical Laboratory Research and Development Service, Department of Veterans Affairs.

Current address for I.J.M.: University of Cincinnati, College of Medicine, 2180 East Galbraith Road, Cincinnati, Ohio 45237.

Disclosure Statement: C.W., B.D., E.A.R., E.B., S.S., S.J.M., M.J.K., A.A.V., H.O. have nothing to declare. I.J.M. was previously employed by Proctor & Gamble Pharmaceuticals. D.B.C. and L.A.E. are employed by Proctor & Gamble Pharmaceuticals. J.S.R. is employed by Proctor & Gamble Pharmaceuticals and holds patents assigned to Proctor & Gamble Pharmaceuticals, but those patents are not relevant to this publication.

REFERENCES

1. Clarke AG, Kendall MD 1994 The thymus in pregnancy: the interplay of neural, endocrine and immune influences. Immunol Today 15:545–551
2. Silverstone AE, Frazier Jr DE, Fiore NC, Soults JA, Gasiewicz TA 1994 Dexamethasone, β-estradiol, and 2,3,7,8-tetrachlorodibenzo-p-dioxin elicit thymic atrophy through different cellular targets. Toxicol Appl Pharmacol 126:248–259
3. Rijhsinghani AG, Thompson K, Bhatia SK, Waldschmidt TJ 1996 Estrogen blocks early T cell development in the thymus. Am J Reprod Immunol 36:269–277
4. Barr IG, Khalid BA, Pearce P, Toh BH, Bartlett PF, Scollay RG, Funder JW 1982 Dihydrotestosterone and estradiol deplete corticosensitive thymocytes lacking in receptors for these hormones. J Immunol 128:2825–2828
5. Hirahara H, Ogawa M, Kimura M, Iiai T, Tsuchida M, Hanawa H, Watanabe H, Abo T 1994 Glucocorticoid independence of acute thymic involution induced by lymphotoxin and estrogen. Cell Immunol 153:401–411
6. Offner H, Polanczyk M 2006 A potential role for estrogen in experimental autoimmune encephalomyelitis and multiple sclerosis. Ann NY Acad Sci 1089:343–372
7. Shames RS 2002 Gender differences in the development and function of the immune system. J Adolesc Health 30:59–70
8. Fuller A, Yahikozawa H, So EY, Dal Canto M, Koh CS, Welsh CJ, Kim BS 2007 Castration of male C57L/J mice increases susceptibility and estrogen treatment restores resistance to Theiler's virus-induced demyelinating disease. J Neurosci Res 85:871–881
9. Aluvihare VR, Kallikourdis M, Betz AG 2004 Regulatory T cells mediate maternal tolerance to the fetus. Nat Immunol 5:266–271
10. Dechering K, Boersma C, Mosselman S 2000 Estrogen receptors α and β: two receptors of a kind? Curr Med Chem 7:561–576
11. Staples JE, Gasiewicz TA, Fiore NC, Lubahn DB, Korach KS, Silverstone AE 1999 Estrogen receptor α is necessary in thymic development and estradiol-induced thymic alterations. J Immunol 163:4168–4174
12. Erlandsson MC, Ohlsson C, Gustafsson JA, Carlsten H 2001 Role of oestrogen receptors α and β in immune organ development and in oestrogen-mediated effects on thymus. Immunology 103:17–25
13. Revankar CM, Cimino DF, Sklar LA, Arterburn JB, Prossnitz ER 2005 A transmembrane intracellular estrogen receptor mediates rapid cell signaling. Science 307: 1625–1630
14. Prossnitz ER, Arterburn JB, Sklar LA 2007 GPR30: a G protein-coupled receptor for estrogen. Mol Cell Endocrinol 265–266:138–142
15. Petrie HT, Hugo P, Scollay R, Shortman K 1990 Lineage relationships and developmental kinetics of immature thymocytes: CD3, CD4, and CD8 acquisition in vivo and in vitro. J Exp Med 172:1583–1588
16. Godfrey DI, Kennedy J, Suda T, Zlotnik A 1993 A developmental pathway involving four phenotypically and functionally distinct subsets of CD3-CD4-CD8- triple-negative adult mouse thymocytes defined by CD44 and CD25 expression. J Immunol 150:4244–4252
17. Saint-Ruf C, Ungewiss K, Groettrup M, Bruno L, Fehling HJ, von Boehmer H 1994 Analysis and expression of a cloned pre-T cell receptor gene. Science 266:1208–1212
18. Ceredig R, Rolink T 2002 A positive look at double-negative thymocytes. Nat Rev Immunol 2:888–897
19. Zoller AL, Kersh GJ 2006 Estrogen induces thymic atrophy by eliminating early thymic progenitors and inhibiting proliferation of β-selected thymocytes. J Immunol 176: 7371–7378
20. Bologa CG, Revankar CM, Young SM, Edwards BS, Arterburn JB, Kiselyov AS, Parker MA, Tkachenko SE, Savchuck NP, Sklar LA, Oprea TI, Prossnitz ER 2006 Virtual and biomolecular screening converge on a selective agonist for GPR30. Nat Chem Biol 2:207–212
21. Aifantis I, Gounari F, Scorrano L, Borowski C, von Boehmer H 2001 Constitutive pre-TCR signaling promotes differentiation through Ca2+ mobilization and activation of NF-κB and NFAT. Nat Immunol 2:403–409
22. Grumont RJ, Rourke IJ, Gerondakis S 1999 Rel-dependent induction of A1 transcription is required to protect B cells from antigen receptor ligation-induced apoptosis. Genes Dev 13:400–411
23. Tamatani M, Che YH, Matsuzaki H, Ogawa S, Okado H, Miyake S, Mizuno T, Tohyama M 1999 Tumor necrosis factor induces Bcl-2 and Bcl-x expression through NFκB activation in primary hippocampal neurons. J Biol Chem 274:8531–8538
24. Van Antwerp DJ, Martin SJ, Verma IM, Green DR 1998 Inhibition of TNF-induced apoptosis by NF-κB. Trends Cell Biol 8:107–111
25. Wang CY, Mayo MW, Korneluk RG, Goeddel DV, Baldwin Jr AS 1998 NF-κB antiapoptosis: induction of TRAF1 and TRAF2 and c-IAP1 and c-IAP2 to suppress caspase-8 activation. Science 281:1680–1683
26. Voll RE, Jimi E, Phillips RJ, Barber DF, Rincon M, Hayday AC, Flavell RA, Ghosh S 2000 NF-κB activation by the pre-T cell receptor serves as a selective survival signal in T lymphocyte development. Immunity 13:677–689
27. Linette GP, Li Y, Roth K, Korsmeyer SJ 1996 Cross talk between cell death and cell cycle progression: BCL-2 regulates NFAT-mediated activation. Proc Natl Acad Sci USA 93:9545–9552
28. Shibasaki F, Kondo E, Akagi T, McKeon F 1997 Suppression of signalling through transcription factor NF-AT by interactions between calcineurin and Bcl-2. Nature 386: 728–731
29. Baeuerle PA, Baltimore D 1988 I κ B: a specific inhibitor of the NF-κB transcription factor. Science 242:540–546
30. Lubahn DB, Moyer JS, Golding TS, Couse JF, Korach KS, Smithies O 1993 Alteration of reproductive function but not prenatal sexual development after insertional disruption of the mouse estrogen receptor gene. Proc Natl Acad Sci USA 90:11162–11166
31. Okasha SA, Ryu S, Do Y, McKallip RJ, Nagarkatti M, Nagarkatti PS 2001 Evidence for estradiol-induced apoptosis and dysregulated T cell maturation in the thymus. Toxicology 163:49–62

32. Do Y, Ryu S, Nagarkatti M, Nagarkatti PS 2002 Role of death receptor pathway in estradiol-induced T-cell apoptosis in vivo. Toxicol Sci 70:63–72
33. Yao G, Hou Y 2004 Thymic atrophy via estrogen-induced apoptosis is related to Fas/FasL pathway. Int Immunopharmacol 4:213–221
34. Zoller AL, Schnell FJ, Kersh GJ 2007 Murine pregnancy leads to reduced proliferation of maternal thymocytes and decreased thymic emigration. Immunology 121: 207–215
35. Kanda N, Watanabe S 2003 17β-Estradiol inhibits oxidative stress-induced apoptosis in keratinocytes by promoting Bcl-2 expression. J Invest Dermatol 121: 1500–1509
36. Kimura M, Mizukami Y, Miura T, Fujimoto K, Kobayashi S, Matsuzaki M 2001 Orphan G protein-coupled receptor, GPR41, induces apoptosis via a p53/Bax pathway during ischemic hypoxia and reoxygenation. J Biol Chem 276:26453–26460
37. Bakker TR, Renno T, Jongeneel CV 1999 Impaired fetal thymocyte development after efficient adenovirus-mediated inhibition of NF-κB activation. J Immunol 162: 3456–3462
38. Zong WX, Edelstein LC, Chen C, Bash J, Gelinas C 1999 The prosurvival Bcl-2 homolog Bfl-1/A1 is a direct transcriptional target of NF-κB that blocks TNFα-induced apoptosis. Genes Dev 13:382–387
39. Krege JH, Hodgin JB, Couse JF, Enmark E, Warner M, Mahler JF, Sar M, Korach KS, Gustafsson JA, Smithies O 1998 Generation and reproductive phenotypes of mice lacking estrogen receptor β. Proc Natl Acad Sci USA 95:15677–15682
40. Bebo Jr BF, Fyfe-Johnson A, Adlard K, Beam AG, Vandenbark AA, Offner H 2001 Low-dose estrogen therapy ameliorates experimental autoimmune encephalomyelitis in two different inbred mouse strains. J Immunol 166: 2080–2089
41. Polanczyk MJ, Hopke C, Vandenbark AA, Offner H 2007 Treg suppressive activity involves estrogen-dependent expression of programmed death-1 (PD-1). Int Immunol 19:337–343
42. Wang C, Mooney JL, Meza-Romero R, Chou YK, Huan J, Vandenbark AA, Offner H, Burrows GG 2003 Recombinant TCR ligand induces early TCR signaling and a unique pattern of downstream activation. J Immunol 171:1934–1940

Molecular Endocrinology **is published monthly by The Endocrine Society (http://www.endo-society.org), the foremost professional society serving the endocrine community.**

CASP7.5
The 2008 between CASP meeting
April 21-23, 2008
Spanish National Cancer Research Centre (CNIO)
Madrid, Spain

CASP7.5 organisers: Michael Tress and Alfonso Valencia.

CASP experiment organisers: John Moult, Krzysztof Fidelis, Andriy Kryshtafovych, Burkhard Rost and Anna Tramontano

Application form: http://www.cnio.es/eventos/index.asp?ev=3

CASP7.5, the second between CASP meeting, will be held in Madrid on April 21-23, 2008.

The focus of the CASP7.5 meeting will be on the progress of structure prediction as measured by the CASP experiments.

There will be presentations on critical areas such as the state of-the-art in structure prediction, model refinement and function prediction.

The CASP7.5 meeting will also focus on CASP-like challenges in other areas of biology.

CASP7.5 is an open meeting and all interested researchers are encouraged to attend.

Participants are invited to submit posters and a number of the presented posters will be selected for short talks.

Conference website: http://casp75.bioinfo.cnio.es/